Electronic supplementary information

Specific chiral recognition of amino acid enantiomers promoted by enzymatic bioreactor in MOFs

Jian Yang,[ab] Yao Jiang,[ab] Guorong Tao*[c] and Jinlou Gu*[ab]

[a]Shanghai Engineering Research Center of Hierarchical Nanomaterials, [b]Key Laboratory for Ultrafine Materials of Ministry of Education, School of Materials Science and Engineering, East China University of Science and Technology, Shanghai 200237, China. [c]Department of Anesthesiology, Ruijin Hospital, Shanghai Jiaotong University School of Medicine, Shanghai 200025, China.

* E-mail: zjsxtgr@126.com (G. R. Tao)

* E-mail: jinlougu@ecust.edu.cn (J. L. Gu).

Fax: +86-21-64250740. Tel: +86-21-64252599 (J. L. Gu)

Chemicals and materials. All amino acid (AA) enantiomers of glutamate (Glu), phenylalanine (Phe), alanine (Ala), cystine (Cys), arginine (Arg), histidine (His), glutamine (Gln), asparagine (Asn), valine (Val), leucine (Leu), lysine (Lys), methionine (Met), aspartic acid (Asp), proline (Pro), serine (Ser), threonine (Thr), tryptophan (Trp), tyrosine (Tyr) and isoleucine (Ile) as well as 3-bromophenol and bis(pinacolato)diboron were obtained from Shanghai D&B Chemical Technology Co., Ltd. N,N-Dimethyl-formamide (DMF) was purchased from Shanghai Meryer Chemical Technology Co., Ltd. L-amino acid oxidase (L-AAO), L-glutamate oxidase (L-GOX) and F127 ($PEO_{106}PPO_{70}PEO_{106}$) were obtained from Sigma-Aldrich. Cerium(IV) ammonium nitrate ($(NH_4)_2Ce(NO_3)_6$) was obtained from Shanghai Macklin Biochemical Co., Ltd. Sodium perchlorate monohydrate ($NaClO_4 \cdot H_2O$) and acetic acid were supplied from Sinpharm Chemical Reagent Co., Ltd. Other chemicals and materials were supplied from Shanghai Titan Technology Co., Ltd. All reagents were of analytical grade, and used without further purification. The applied water (18.1 $M\Omega \cdot cm^{-1}$) in the experiments was purified from a NW Ultrapure Water System (Heal Force, China).

Instruments and methods. The powder X-ray diffraction (XRD) patterns were obtained on a Bruker D8 instrument using Cu Kα radiation (40 kV, 40 mA). SEM images were observed on a JEOL JSM-6700F microscope. Nuclear magnetic resonance (NMR) spectra were obtained through an AVANCE III 400 instrument. The surface area was measured on a surface area and porosity analyzer (Micromeritics, TriStar II) equipped with a sample degassing system (Micromeritics, VacPrep 061) via calculation

with the Brunauer-Emmett-Teller (BET) method. All of the samples were degassed under vacuum at 120 °C for 12 h prior to analysis. The UV-Vis absorption spectra were measured with a UV-3600 spectrophotometer (Shimadzu, Tokyo, Japan). The fluorescence spectra were recorded with an RF-5301PC spectrophotometer (Shimadzu). The standard CIF file of the UiO-66(Ce) structure has been provided in the original work of Stock *et al.*,[1] and has been deposited with the Cambridge Crystallographic Data Center (CCDC 1036904). Therefore, the crystal structure of pristine UiO-66(Ce) was used as starting model for the Rietveld refinement of PXRD data of OMUiO-66(Ce), and the refinement was performed using TOPAS academics.[2]

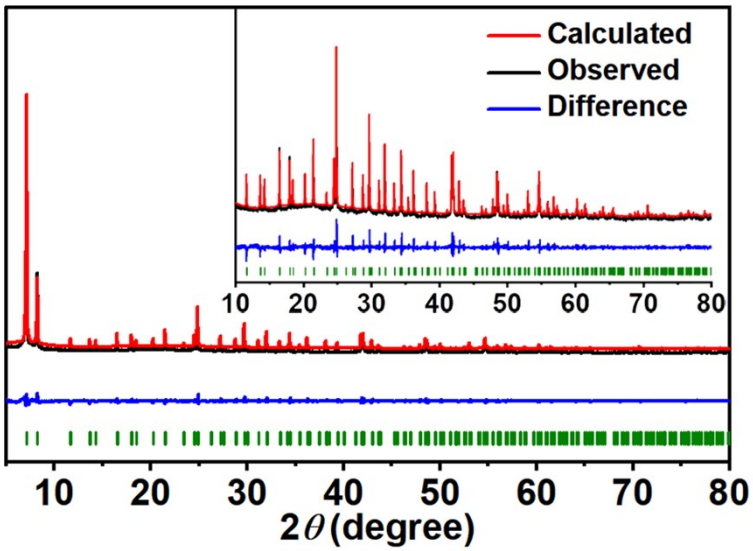

Fig. S1 Rietveld refinement for the OMUiO-66(Ce) using a fixed occupancy factor for the linker molecule. The observed PXRD pattern (λ = 1.5401 Å) (black), the calculated curve (red) and the difference plot (blue) are shown. The allowed peak positions are marked as green ticks. The inset picture is the enlarged region between 10° to 80°.

Table S1 Comparison of crystallographic data of OMUiO-66(Ce) and the reported UiO-66(Ce).

	UiO-66(Ce)[1]	OMUiO-66(Ce)
Wavelength /Å	$CuK\alpha_1$	$CuK\alpha_1$
***a* /Å**	21.4727(3)	21.5020(7)
Crystal system	Cubic	Cubic
Space group	$Fm\bar{3}m$	$Fm\bar{3}m$
Volume /Å^3	9900.6(4)	9941.2(4)
R_{wp} / %	2.65	10.280
R_p / %	5.86	7.757
GoF	2.268	2.896

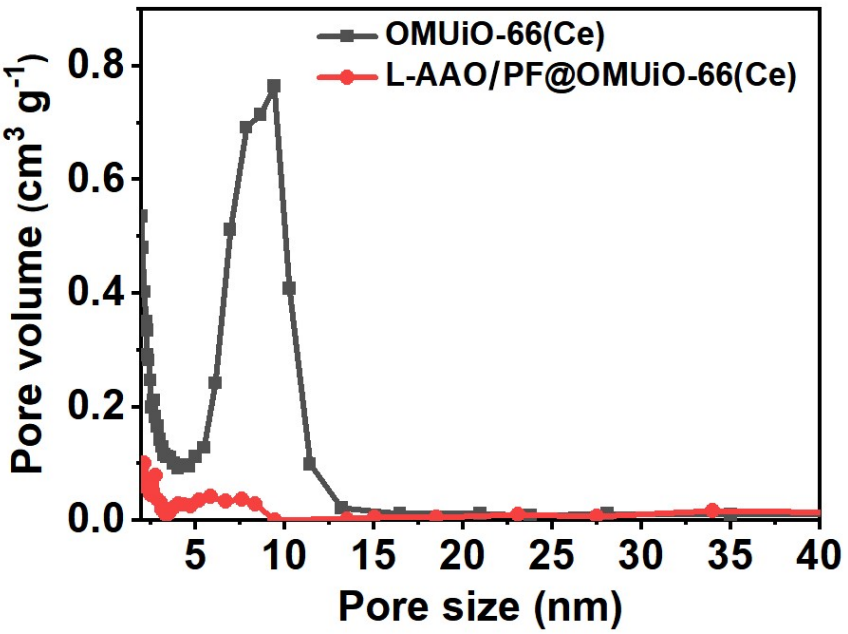

Fig. S2 The corresponding pore size distribution of OMUiO-66(Ce) (Black line) and L-AAO/PF@OMUiO-66(Ce) (Red line).

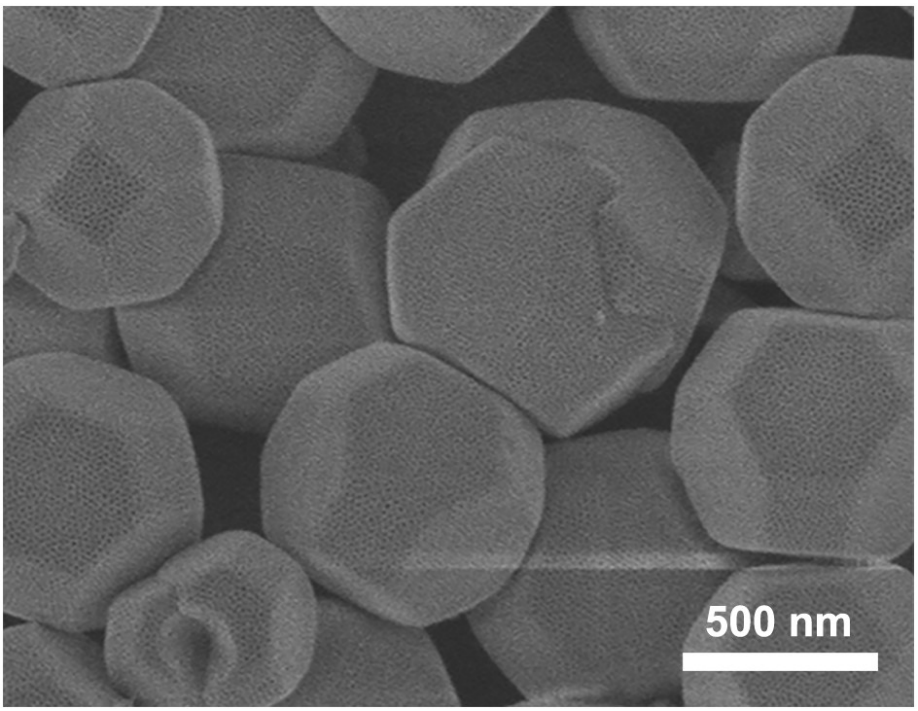

Fig. S3 SEM image of the large scale of OMUiO-66(Ce) demonstrated that mesochannels were distributed on each particle.

Table S2 Textural parameters for the as-synthesized OMUiO-66(Ce) and L-AAO/PF@OMUiO-66(Ce).

Samples	D_{meso} (nm)	S_{BET} (m^2/g)	V_P (cm^3/g)
OMUiO-66(Ce)	9.4	994	0.542
L-AAO/PF@OMUiO-66(Ce)	6.7	263	0.142

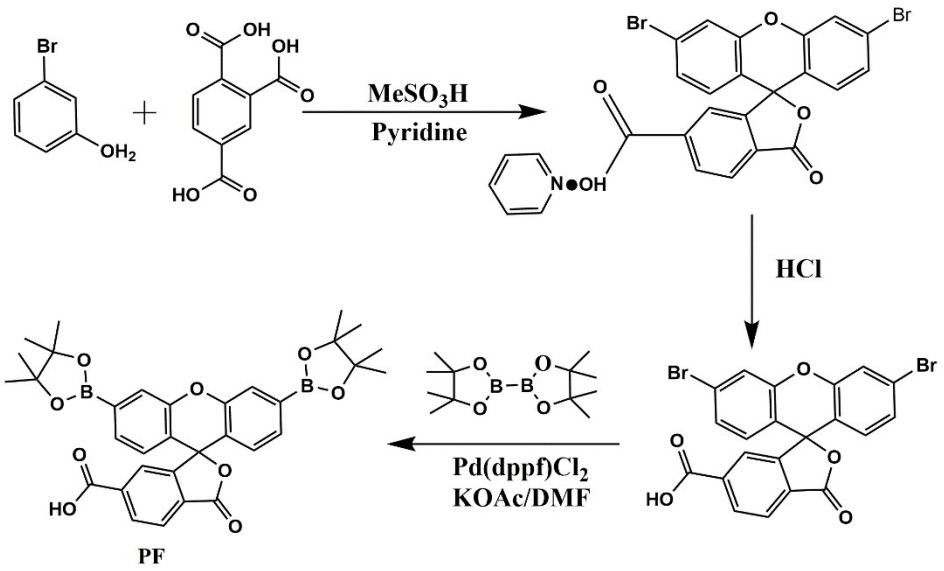

Scheme S1 Synthesis route for the carboxyl-functionalized boronate esters compound of PF.

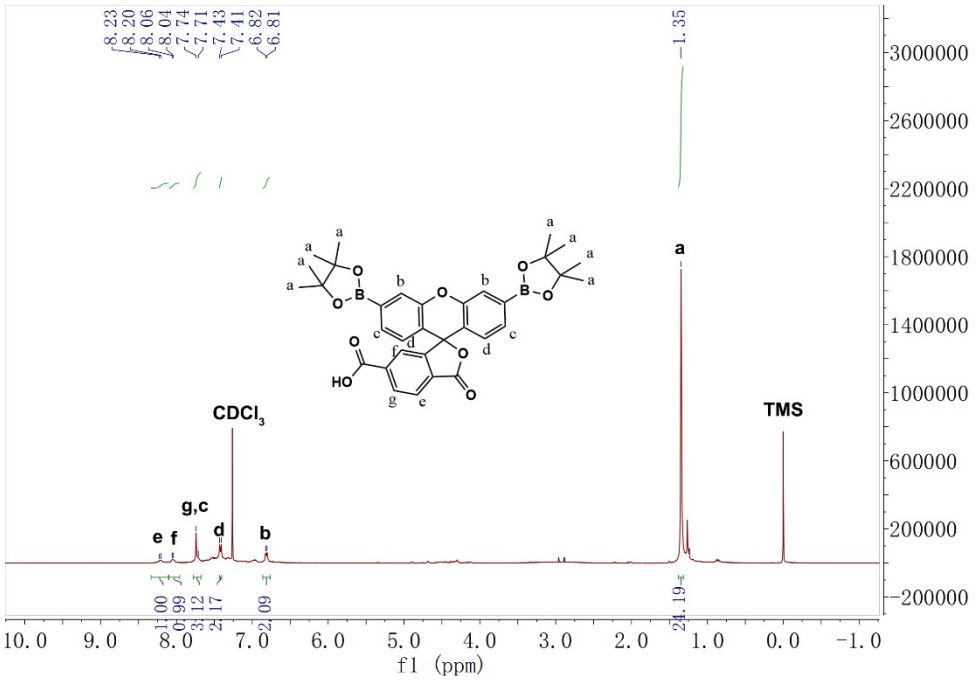

Fig. S4 ^{1}H NMR ($CDCl_3$) spectrum of 3-Oxo-3',6'-bis(4,4,5,5-tetramethyl-1,3,2-dioxaborolan-2-yl)-3H-spiro[isobenzofuran-1,9'-xanthene]-6-carboxylic acid (PF). ^{1}H NMR ($CDCl_3$, 400 MHz): δ 8.23 (d, 1H), 8.06 (d, 1H), 8.01 (1H, s), 7.74 (m, 3H), 7.43 (d, 2H), 6.82 (d, 2H), 1.35 (s, 24H).

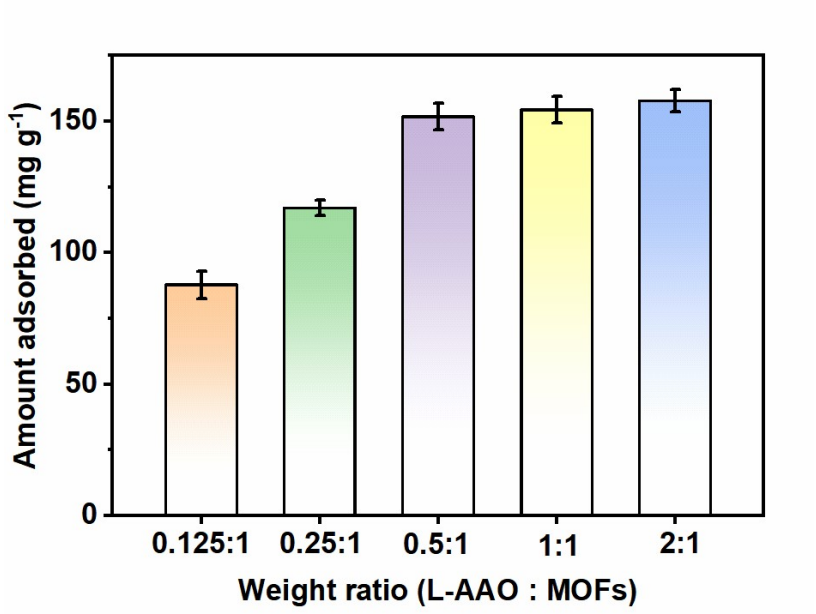

Fig. S5 Loading amounts of L-AAO in OMUiO-66(Ce). The initial weight ratios of L-AAO to MOFs are 0.125:1 (orange), 0.25:1 (green), 0.5:1 (violet), 1:1 (yellow) and 2:1 (blue).

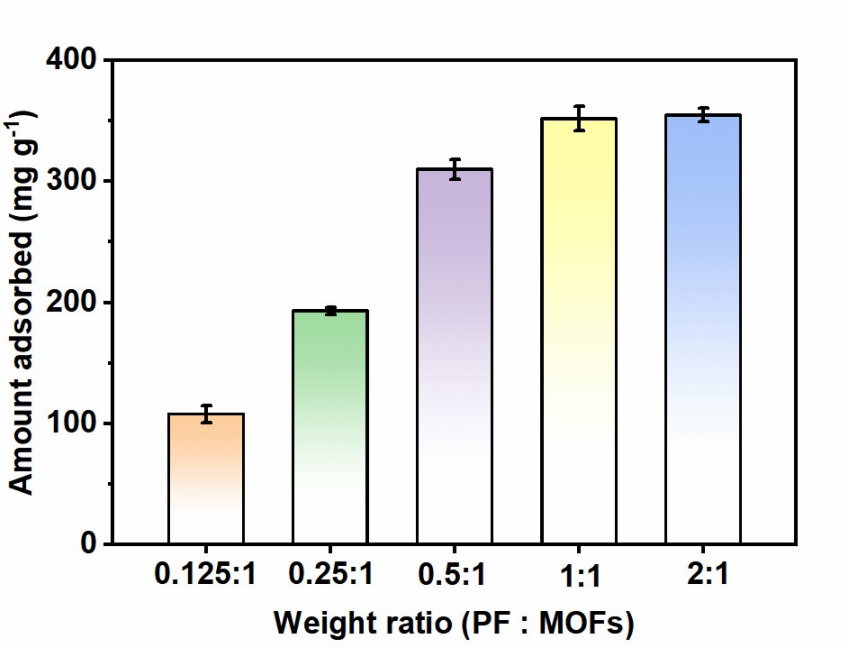

Fig. S6 Loading amounts of PF in L-AAO@OMUiO-66(Ce). The initial weight ratios of PF to MOFs are 0.125:1 (orange), 0.25:1 (green), 0.5:1 (violet), 1:1 (yellow) and 2:1 (blue).

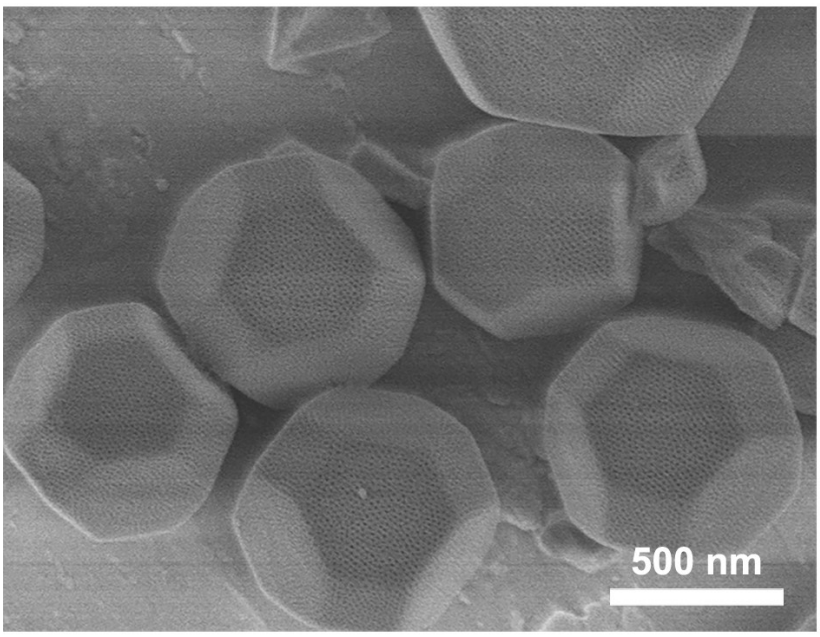

Fig. S7 SEM image of the magnified L-AAO/PF@OMUiO-66(Ce) particles.

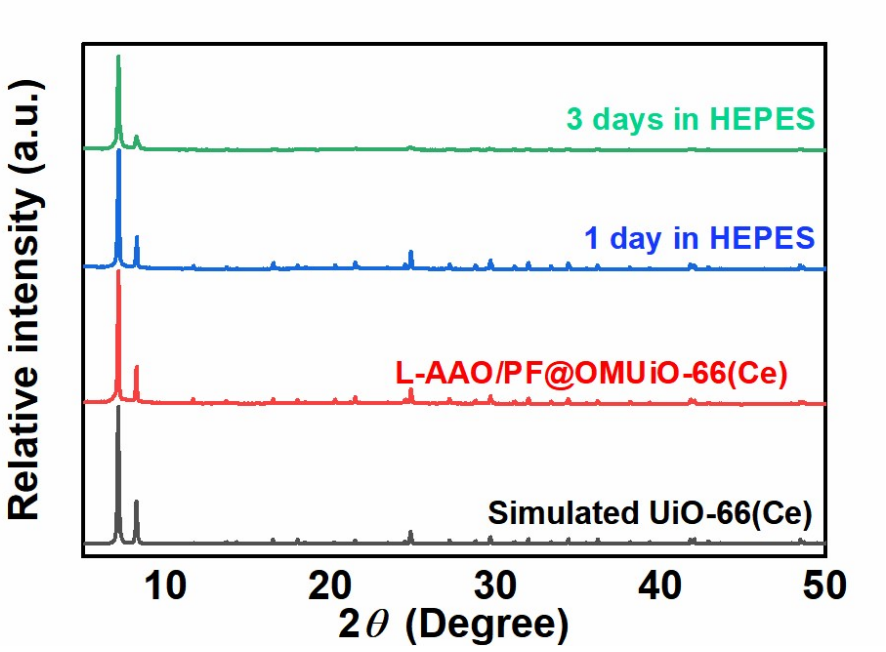

Fig. S8 XRD patterns of the simulated UiO-66(Ce) structure, the as-synthesized samples of L-AAO/PF@OMUiO-66(Ce), and L-AAO/PF@OMUiO-66(Ce) upon the treatments in HEPES buffer solution (pH = 7.4) for 1 day and 3 days for the test of the structural stability.

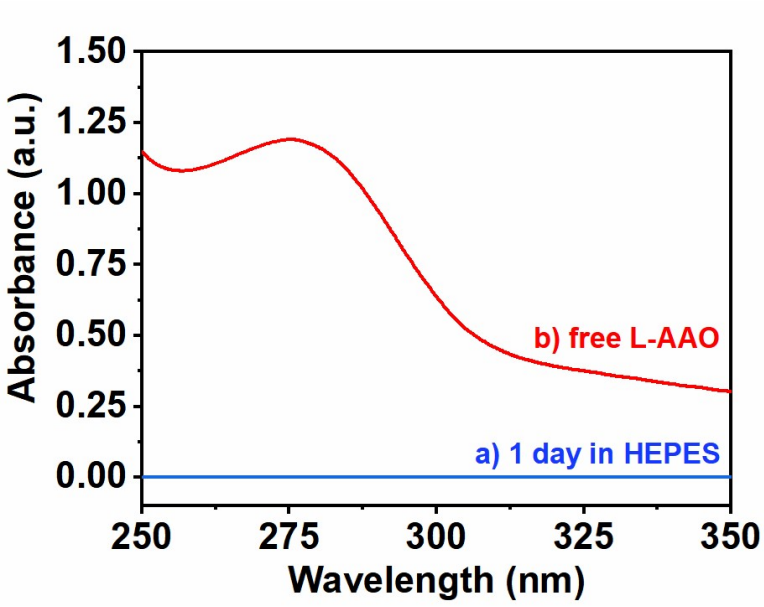

Fig. S9 The UV−Vis absorption spectra of (a) the supernatant of L-AAO/PF@OMUiO-66(Ce) in HEPES buffer solution (pH = 7.4) for 1 day and (b) free L-AAO solution.

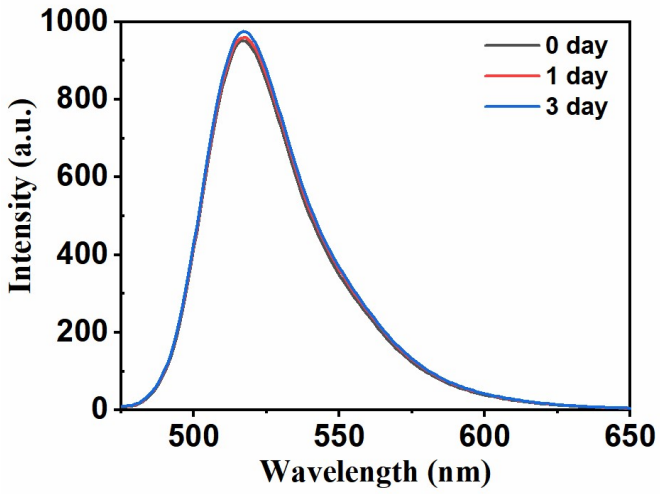

Fig. S10 The "turn-on" fluorescent spectra of L-AAO/PF@OMUiO-66(Ce) probe for its response to 100 μM L-Phe (Black line) and its preservation in HEPES buffer solution (pH = 7.4) for 1-3 days (Red and blue lines).

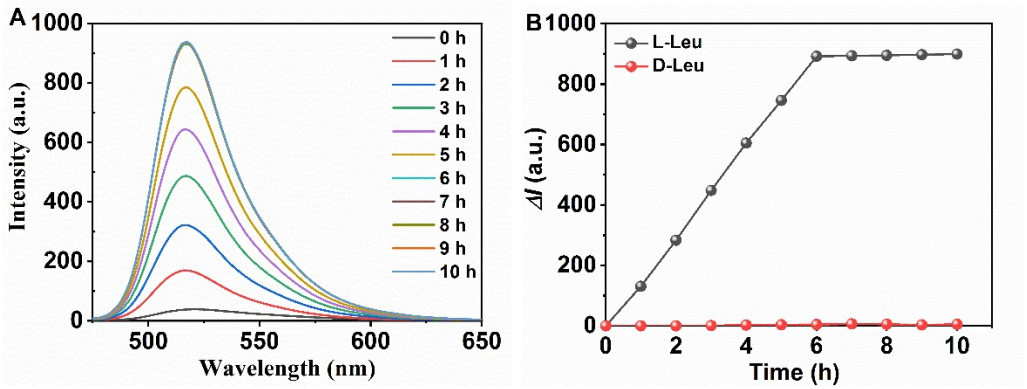

Fig. S11 (A) Fluorescence spectra of L-AAO/PF@OMUiO-66(Ce) suspension (100 mg L^{-1}, pH = 7.4) upon the addition of L-Leu (100 μM) under various incubation time. (B) The comparison of kinetics fluorescence response of probe towards L- Leu and D- Leu (100 μM).

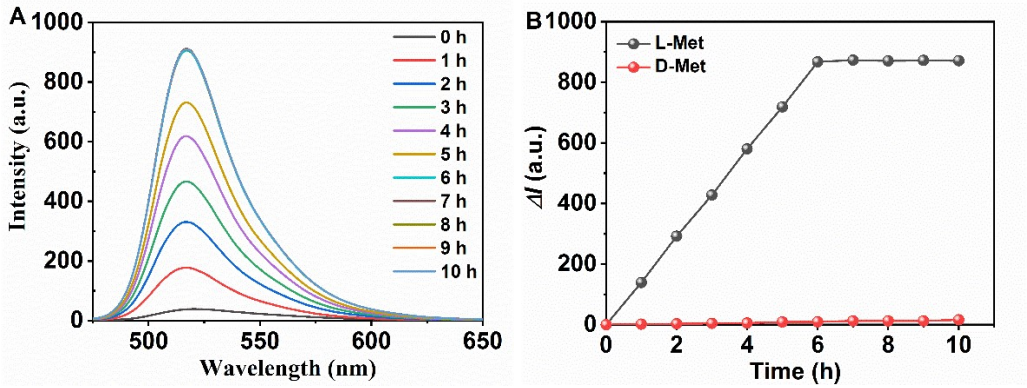

Fig. S12 (A) Fluorescence spectra of L-AAO/PF@OMUiO-66(Ce) suspension (100 mg L^{-1}, pH = 7.4) upon the addition of L-Met (100 μM) under various incubation time. (B) The comparison of kinetics fluorescence response of probe towards L-Met and D-Met (100 μM).

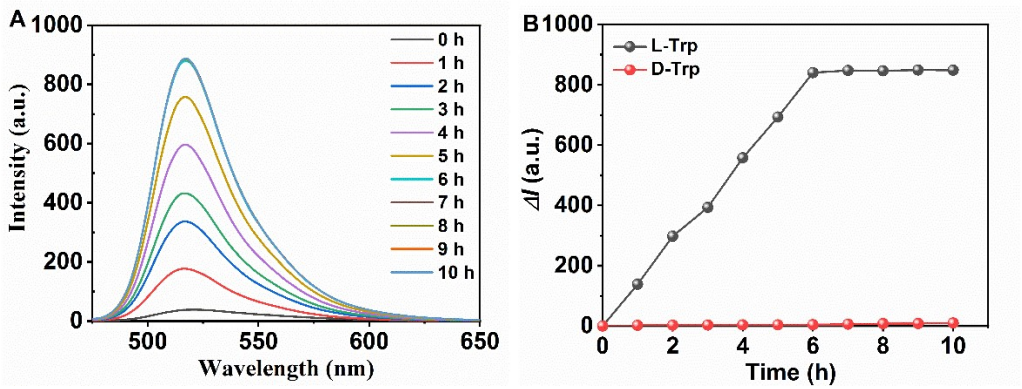

Fig. S13 (A) Fluorescence spectra of L-AAO/PF@OMUiO-66(Ce) suspension (100 mg L^{-1}, pH = 7.4) upon the addition of L-Trp (100 μM) under various incubation time. (B) The comparison of kinetics fluorescence response of probe towards L-Trp and D-Trp (100 μM).

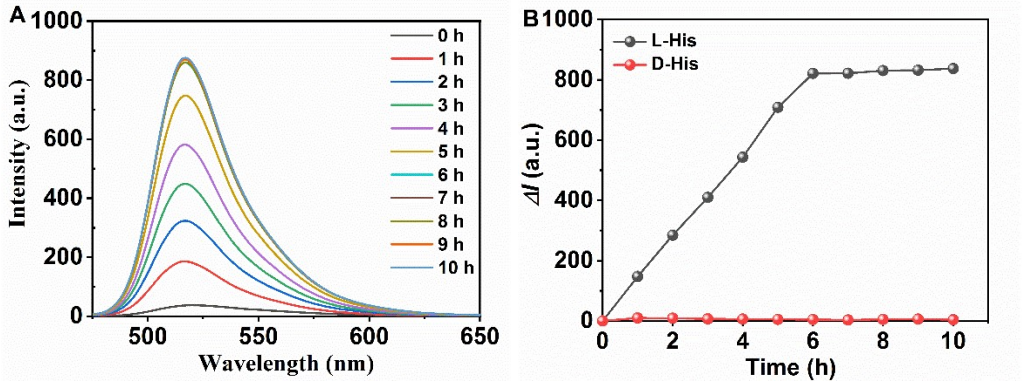

Fig. S14 (A) Fluorescence spectra of L-AAO/PF@OMUiO-66(Ce) suspension (100 mg L^{-1}, pH = 7.4) upon the addition of L-His (100 μM) under various incubation time. (B) The comparison of kinetics fluorescence response of probe towards L-His and D-His (100 μM).

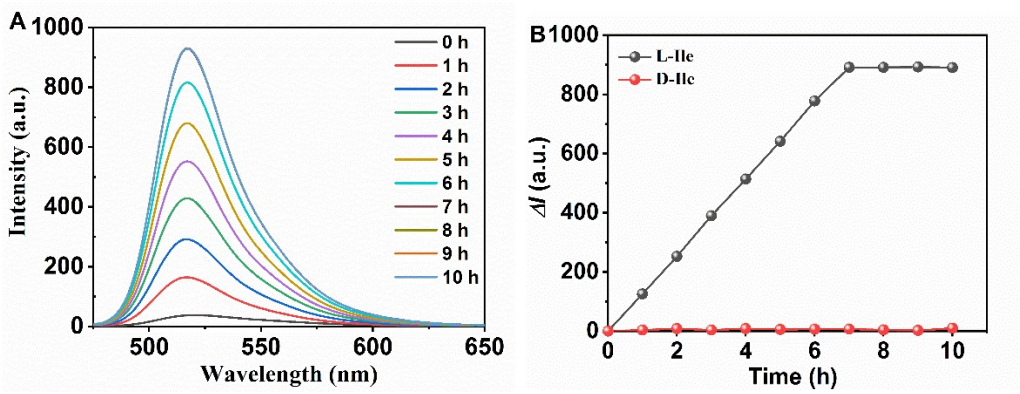

Fig. S15 (A) Fluorescence spectra of L-AAO/PF@OMUiO-66(Ce) suspension (100 mg L^{-1}, pH = 7.4) upon the addition of L-Ile (100 μM) under various incubation time. (B) The comparison of kinetics fluorescence response of probe towards L-Ile and D-Ile (100 μM).

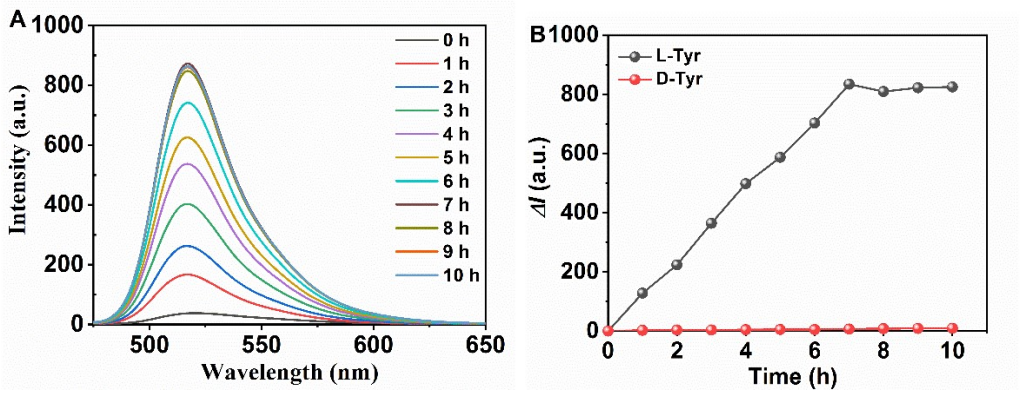

Fig. S16 (A) Fluorescence spectra of L-AAO/PF@OMUiO-66(Ce) suspension (100 mg L^{-1}, pH = 7.4) upon the addition of L-Tyr (100 μM) under various incubation time. (B) The comparison of kinetics fluorescence response of probe towards L-Tyr and D-Tyr (100 μM).

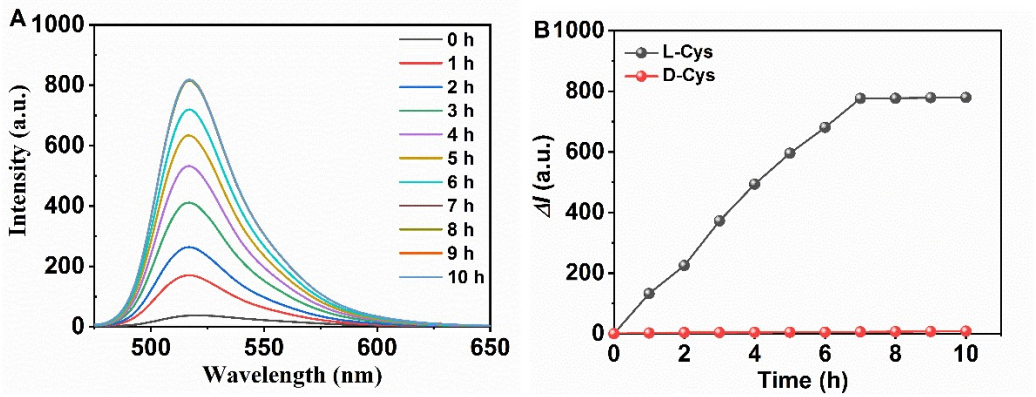

Fig. S17 (A) Fluorescence spectra of L-AAO/PF@OMUiO-66(Ce) suspension (100 mg L^{-1}, pH = 7.4) upon the addition of L-Cys (100 μM) under various incubation time. (B) The comparison of kinetics fluorescence response of probe towards L-Cys and D-Cys (100 μM).

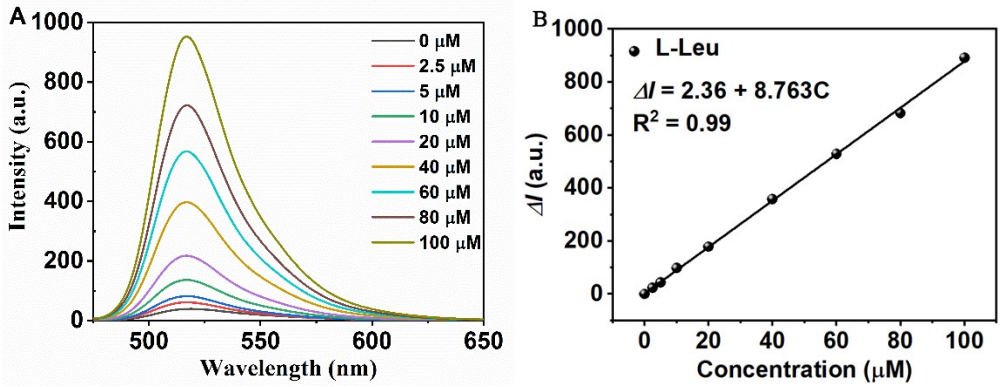

Fig. S18 (A) Evolvement of the fluorescence spectra of L-AAO/PF@OMUiO-66(Ce) (100 mg L^{-1}) suspension in HEPES buffer solution (pH = 7; 20 mM) upon the addition of various concentrations of L-Leu. (B) The corresponding Linear fitting plot of the enhanced fluorescence intensity of probe as a function of the concentration of L-Leu.

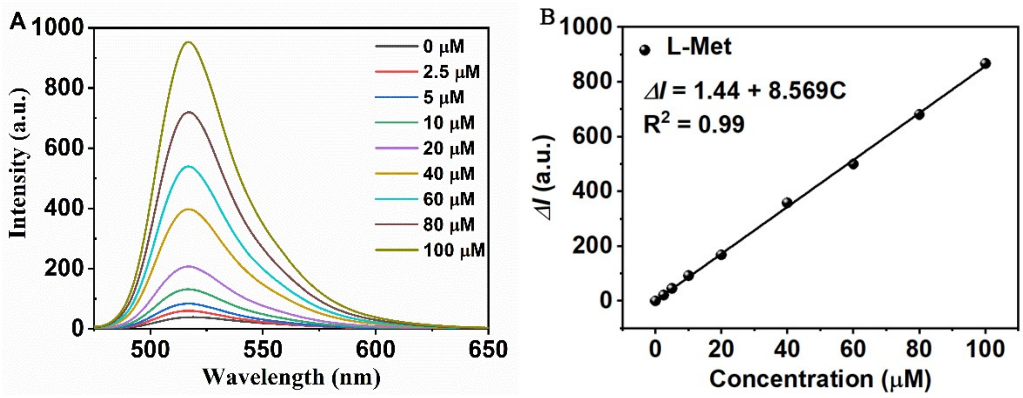

Fig. S19 (A) Evolvement of the fluorescence spectra of L-AAO/PF@OMUiO-66(Ce) (100 mg L^{-1}) suspension in HEPES buffer solution (pH = 7; 20 mM) upon the addition of various concentrations of L-Met. (B) The corresponding Linear fitting plot of the enhanced fluorescence intensity of probe as a function of the concentration of L-Met.

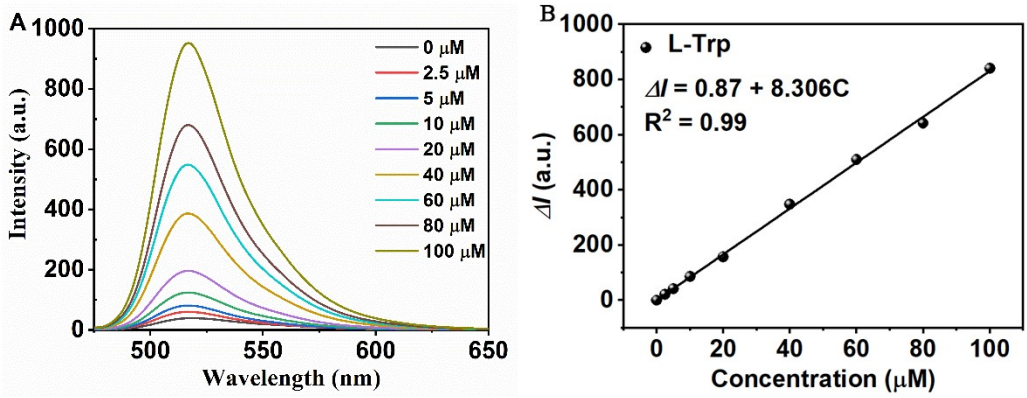

Fig. S20 (A) Evolvement of the fluorescence spectra of L-AAO/PF@OMUiO-66(Ce) (100 mg L^{-1}) suspension in HEPES buffer solution (pH = 7; 20 mM) upon the addition of various concentrations of L-Trp. (B) The corresponding Linear fitting plot of the enhanced fluorescence intensity of probe as a function of the concentration of L-Trp.

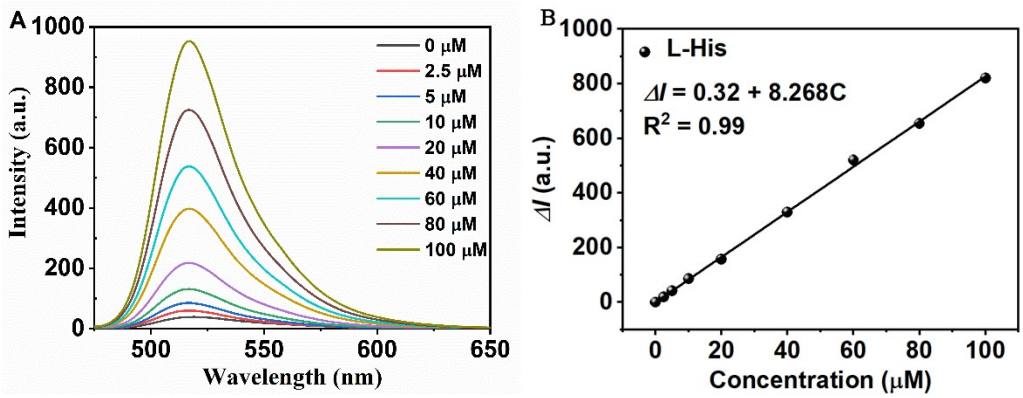

Fig. S21 (A) Evolvement of the fluorescence spectra of L-AAO/PF@OMUiO-66(Ce) (100 mg L^{-1}) suspension in HEPES buffer solution (pH = 7; 20 mM) upon the addition of various concentrations of L-His. (B) The corresponding Linear fitting plot of the enhanced fluorescence intensity of probe as a function of the concentration of L-His.

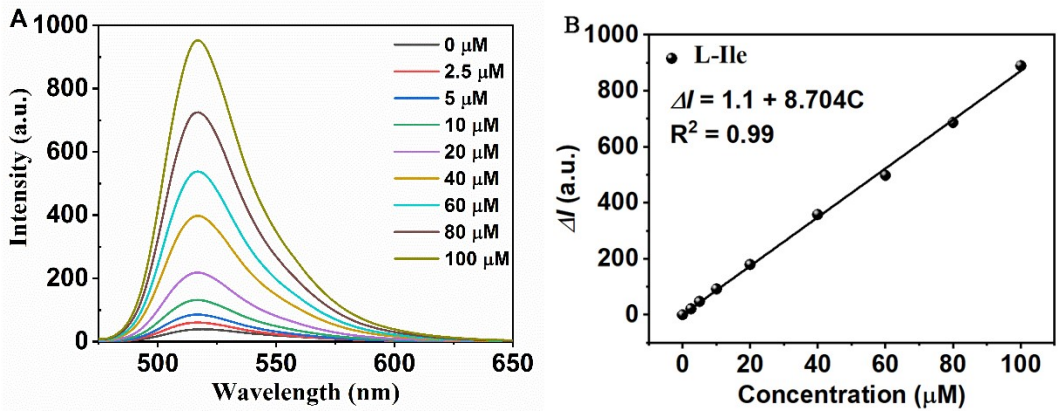

Fig. S22 (A) Evolvement of the fluorescence spectra of L-AAO/PF@OMUiO-66(Ce) (100 mg L^{-1}) suspension in HEPES buffer solution (pH = 7; 20 mM) upon the addition of various concentrations of L-Ile. (B) The corresponding Linear fitting plot of the enhanced fluorescence intensity of probe as a function of the concentration of L-Ile.

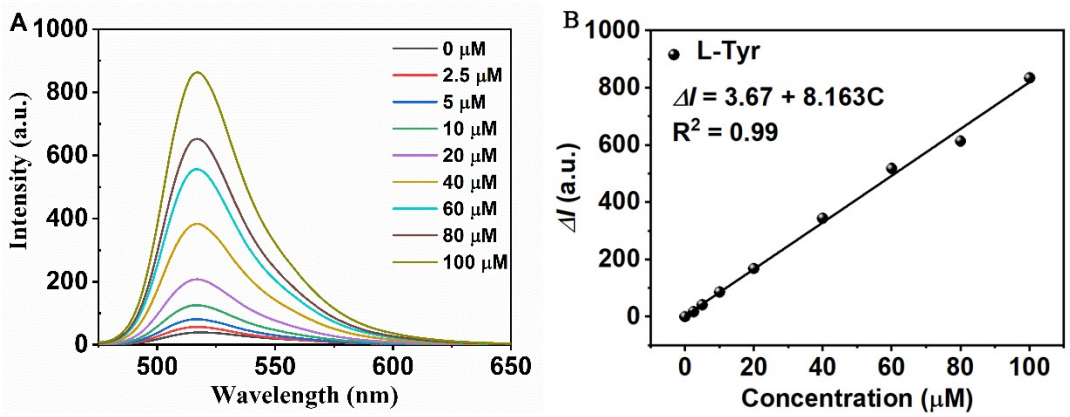

Fig. S23 (A) Evolvement of the fluorescence spectra of L-AAO/PF@OMUiO-66(Ce) (100 mg L^{-1}) suspension in HEPES buffer solution (pH = 7; 20 mM) upon the addition of various concentrations of L-Tyr. (B) The corresponding Linear fitting plot of the enhanced fluorescence intensity of probe as a function of the concentration of L-Tyr.

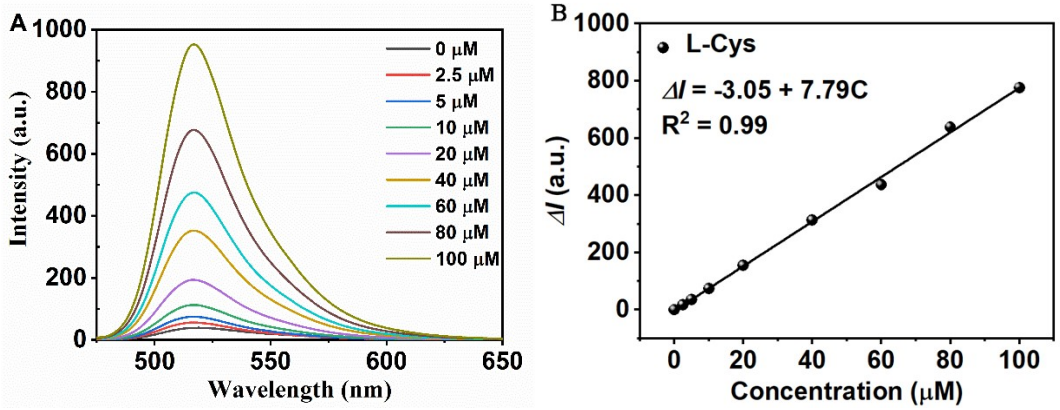

Fig. S24 (A) Evolvement of the fluorescence spectra of L-AAO/PF@OMUiO-66(Ce) (100 mg L^{-1}) suspension in HEPES buffer solution (pH = 7; 20 mM) upon the addition of various concentrations of L-Cys. (B) The corresponding Linear fitting plot of the enhanced fluorescence intensity of probe as a function of the concentration of L-Cys.

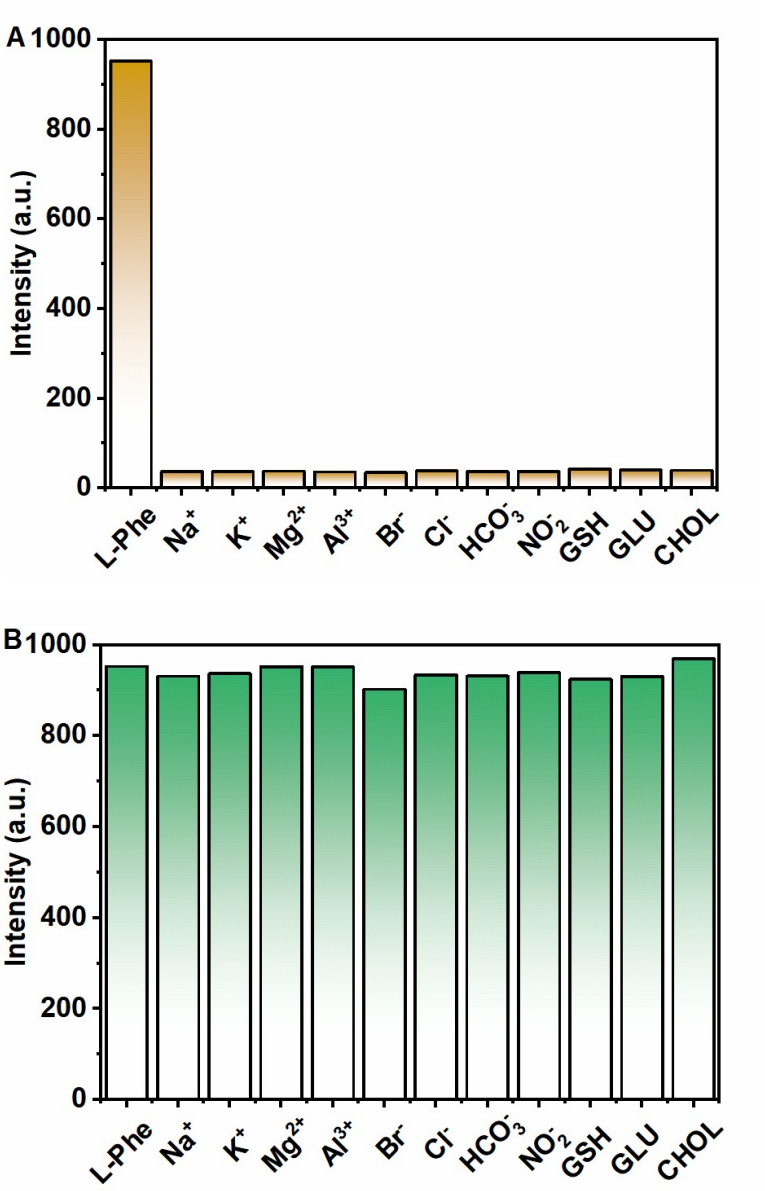

Fig. S25 (A) The fluorescence response of L-AAO/PF@OMUiO-66(Ce) (100 mg L^{-1}, pH = 7.4) suspension towards L-Phe (100 μM) and other possible interfering compounds (1000 μM). (B) The fluorescence response of L-AAO/PF@OMUiO-66(Ce) (100 mg L^{-1}, pH = 7.4) suspension towards L-Phe (100 μM) in the presence of various coexistent interfering compounds (1000 μM).

Table S3 The comparison of sensing features between the developed probes and other reported fluorescent probes for the detection of AA enantiomers.

Chiral selector	Enantio/chemo-selectivity[a]	Sensing system	*ef*[b]	Linear range (μM)	LOD (μM)	Analytes	Ref.
1,1′-binaphthyl derivatives	Yes	Aqueous phase	1.65	0-100	2.6	Trp	*3*
	No	Organic phase	89-199	0-40	-	Ala, Leu, Val, Met, Phe,	*4*
	No	Organic phase	-	0-20	-	Ala, Leu, Ser, Phe, Met, Thr	*5*
	No	Organic phase	-	40-280	-	Phe, Ala, Ser, His, Glu	*6*
	No	Organic pahse	< 13	0-60	-	Phe, His, Leu, Ser, Val	*7*
Quantum dots	Yes	Aqueous Phase	-	150-20000	300	Lys	*8*
Cyclodextrin	No	Organic phase	1.5-5.3	-	-	Phe, Pro, Leu, Val, Ser, Tyr	*9*
L-AAO	No	Aqueous Phase	91-213	0-100	0.38-0.44	Phe, Leu, Met, Trp, His, Ile, Tyr, Cys	*This work*
L-GOX	Yes	Aqueous Phase	187	0-100	0.39	Glu	*This work*

[a]Enantio/chemoselectivity represent the achievement of both enantioselective and chemoselective recognition of a specific AA enantiomer among numerous AAs. [b]*ef* ($\Delta I_L/\Delta I_D$ or $\Delta I_D/\Delta I_L$) represent the enantioselective enhancement ratios of probes between L-AA and its corresponding D-AA.

Table S4 Detection of L-Phe from mixed amino acid enantiomers in SBF samples using L-AAO/PF@OMUiO-66(Ce) probe (n = 4[a]).

Samples	Added (μM)	Measured (μM) ± σ[b]	Recovery (%)[c]	RSD (%)[d]
L-Phe/D-Phe	5/100	5.2 ± 0.3	104	5
L-Phe/D-Phe	20/100	19.6 ± 0.6	98	3
L-Phe/D-Phe	40/100	41.6 ± 0.5	104	1
L-Phe/D-Phe	60/100	60.4 ± 1.0	101	2

[a] n is the repetitive measurement number. [b] Standard derivations are calculated based on 4 times repeated measurements. [c] Recovery (%) = ($C_{mean\ detected}/C_{added\ analyte}$)*100. [d] RSD (%) = ($\sigma/C_{mean\ detected}$)*100.

References

1 M. Lammert, M. T. Wharmby, S. Smolders, B. Bueken, A. Lieb, K. A. Lomachenko, D. D. Vos and N. Stock, *Chem. Commun.,* 2015, **51**, 12578.

2 Topas Academics 4.2, Coelho Software 2007.

3 G. Du, Y. Mao, M. A. Abed and L. Pu, *Mater. Chem. Front,* 2020, **4**, 2384.

4 Y.-Y. Zhu, X.-D. Wu, S.-X. Gu and L. Pu, *J. Am. Chem. Soc.,* 2019, **141**, 175.

5 C. Zeng, X. Zhang and L. Pu, *Chem. -Eur. J.,* 2017, **23**, 2432.

6 K. Wen, S. Yu, Z. Huang, L. Chen, M. Xiao, X. Yu and L. Pu, *J. Am. Chem. Soc.,* 2015, **137**, 4517.

7 Z. Huang, S. Yu, K. Wen, X. Yu and L. Pu, *Chem. Sci.,* 2014, **5**, 3457.

8 F. Copur, N. Bekar, E. Zor, S. Alpaydin and H. Bingol, *Sens. Actuators B,* 2019, **279**, 305.

9 S. Pagliari, R. Corradini, G. Galaverna, S. Sforza, A. Dossena, M. Montalti, L. Prodi, N. Zaccheroni and R. Marchelli, *Chem. Eur. J.,* 2004, **10**, 2749.